Applied Science, Engineering and Management Bulletin [ASEMB]
ISSN: 3049-3005
Vol. 3 No. 03 (July-Sep) (2026) Pg: 114-122

Low Temperature Synthesis Structural and Magnetic properties of Lanthanum Ferrite ($Lafeo_3$) Nanoparticles.

Kumar Sanjay Sinha[1], Dr. Rohit kumar[2], Dr. Arun kumar singh[3]
[1]Government Engineering College West Champaran Bihar, krsanjaysinha121@gmail.com
[2]G E C Gopalganj Bihar, rkroy190@gmail.com
[3]Department of Physics, L.N.M.U., Darbhanga -846008, India

Abstract

We are going to study about the Phase pure nanosized Orthorhombic $LaFeO_3$ powder is synthesized by Sol-Gel auto combustion method. This method is most efficient and time saving compared to other method. The precursors used for the synthesis are Metal nitrates as metal source and propylene glycol as chelating agent and distilled water (DW) as solvent. The formation mechanism, crystal structure, Phase composition, crystallinity, particle size and magnetic properties are investigated by thermogravimetry analysis (TGA), differential scanning calorimetry (DSC), infrared spectroscopy, X-Ray photoelectron microscopy (XPS), transmission electron microscopy (TEM), X-Ray diffraction (XRD), Raman spectroscopy, and SQUID magnetometry. The TGA/DSC confirms the phase formation is completed at 600^0C. XRD data confirms the formation of Phase pure nanocrystalline $LaFeO_3$ with crystallite size of 23 nm. The average particle size is obtained by TEM which is 42nm. Ring shape SAED pattern suggest the polycrystalline nature of sample. The magnetic propertiesare investigatedat 5K and 300K.$LaFeO_3$ nanoparticles shows weak ferromagnetic property at room temperature dueto size-confinement effects with saturation magnetization (M_s) = 0.96 emu/gm, remanence (M_r)=0.06 emu/gm, and Coercivity (H_c)=1776Oe.

Keywords: *Sol-gel synthesis, nanoparticles, X-ray diffraction, Magnetism*

1. Introduction:

Multifunctional rare-earth ortho ferrites (ABO_3, A= La, Pr, Nd, Sm, Er, Gd etc.) have found useful applications in electrode material for fuel cell, chemical sensors, environmental catalyst, nonvolatile magnetic memory devices, and ultrasensitive magnetic read heads of modern hard disk drives,[**1-7]**. Among the various rare-earth-orthoferrites, lanthanum orthoferrite ($LaFeO_3$) have attracted much attention due to its room temperature (RT) multiferroic behaviour i.e., simultaneous co-existence of coupled magnetic and electric orderings at room temperature [7] In recent years, magnetoelectric multiferroics have been studies exhaustively [8-16] $LaFeO_3$ normally crystallizes in a distorted perovskite structure with an orthorhombic unit cell ($a \neq b \neq c$, α, β and $\gamma = 90$) with a space group of Pbnm. The lattice parameters are a=5.557 Å, b=5.565 Å and c=7.854 Å [15,16,17]. In the perovskite structure, the Fe^{3+} ion is surrounded by six O^{2-} ions and forms an octahedron. Neutron diffraction studies have shown that $LaFeO_3$ exhibits canted G-type antiferromagnetic structure (AFM) with high Ne'el temperature (TN ~740 K) in which each Fe^{3+} is surrounded by six antiparallel Fe^{3+} nearest neighbours [18]. Basically, the stability of the perovskite structure ABO_3 (A = rare earth ion) depends on the tolerance factor (t)[19-20]. In case of $LaFeO_3$, the value of this factor "t" is less than 1 which implies that the cubic structure transforms to orthorhombic structure and hence the Fe-O-Fe bond angle deviates from 180o which leads to a distortion in FeO_6 octahedron. Consequently, the properties of $LaFeO_3$ can be tuned precisely by taking different steps, which include (i) decrease in particle size of $LaFeO_3$ and (ii) doping of La and/or Fe-sites The properties of $LaFeO_3$ can be tuned by controlling surface to volume ratio or particle size [21-24.] The nanoscale $LaFeO_3$ will show different properties from its bulk counterpart. Therefore, synthesis of nanostructures offers great potential to enhance the physical properties and widen the potential applications of $LaFeO_3$. Conventionally, $LaFeO_3$ is prepared by high temperature solid state reactions methods using metal oxides as starting materials. This process suffers with several problems, e.g., poor homogeneity and high porosity of the samples, no control on the particle size, high sintering temperature etc [25-27] It has been established that the size and shape-controlled synthesis is gaining tremendous interest in nanostructure materials research [27-28] The development of revolutionary synthesis procedures through chemistry has made it possible to lower the preparation temperature and to improve homogeneity and reproducibility of the products with the synthesis of ultrafine and chemically pure powders of

mixed-metal oxides at low temperatures. So far, synthesis of phase pure nanosized LaFeO3 has been attempted by variety of wet chemical methods such as hydrothermal synthesis [28-32] auto combustion, sol–gel [33-34] microwave-assisted method [35-36] sonochemical synthesis [37] polymerization complex method [38-39] microemulsion method [40] and tartaric acid method [41] Some of these wet chemical methods, however, lead to nearly phase pure LaFeO3 with traces of secondary phases and some need calcining at relatively high temperature in order to obtain the desired final powders with good crystal structure.. In this work, a low temperature modified sol-gel method is proposed to synthesize phase pure perovskite LaFeO3 nanoparticles. The synthesized samples were characterized by X-ray diffraction, Scanning Electron Microscopy, Transmission Electron Microscopy, Raman. The magnetic properties of pure and doped LaFeO3 will be studied by using Physical Property Measurement System (PPMS) or Superconducting Quantum interference Device (SQUID)

2. Experimental techniques and synthesized samples

For the synthesis of $LaFeO_3$ nanoparticles, lanthanum nitrate hexahydrate ($La(NO_3)_3$.$6H_2O$, Sigma Aldrich, 99.9%) and ferric nitrate nonahydrate, $Fe(NO_3)_3.9H_2O$ (Sigma Aldrich, 99.9%), propylene glycol(Thermo Fisher, India) were used and all are of analytical grade. Lanthanum Nitrate and Iron nitrate are separately dissolved in distilled water in appropriate stoichiometric amount and mixed to obtain precursor solution. Now the complexing agent propylene glycol in 1:1 molar ratio with respect to Metals is added to this precursor solution under constant stirring. This solution is thoroughly stirred and heated at about ~100 ºC till the all liquid is evaporated out from the solution and gel-like solution is formed. Further, this gel-like solution is transformed in puffy precursor powder. Now, this precursor powder is calcined in muffle furnace at 550ºC temperatures for 2h to get well crystallized $LaFeO_3$ nanoparticles. The preparation scheme is illustrated schematically in Figrange from 10° to 90°.

3. Results and discussion:

Structural analysis

The XRD patterns of the prepared $LaFeO_3$ precursor and powders LFO calcined at 450º–600ºC for 2h is shown in (fig.1) The prepared $LaFeO_3$ precursor is XRD amorphous, as is characterized by the broad continuum. At 450º C, some weak XRD peaks showed up in addition to the continuum, which correspond to reflections from $LaFeO_3$. Heating the precursors to 500ºC yields pure orthorhombic $LaFeO_3$with a perovskite structure, and the XRD patterns are in excellent accord with ICCD file 8. The XRD analysis did not show any secondary phases of $LaFeO_3$. Increasing the calcination temperature to 500ºC and 550º C, the diffraction peaks become stronger and sharper, reflecting greater crystallization. No other significant changes are observed and all diffraction lines could be indexed to the orthorhombic structure of $LaFeO_3$. Therefore, single-phase $LaFeO_3$was completely crystallized into the perovskite phase at a temperature as low as 500ºC.

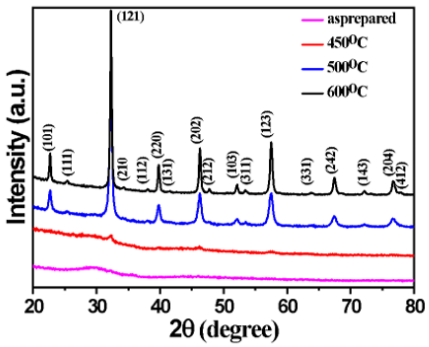


Fig. 1(a): X-Ray Diffraction(XRD) patterns of $LaFeO_3$ (LFO) powders calcined at different temperatures

Figure (1) shows XRD pattern of as prepared LFO precursor powder and LFO powder calcined at different temperatures. After performing calcinations at different temperature phase formation of LFO is completed at 550ºC. All the diffraction peaks is indexed with JCPDS. As it observed, lanthanum ferrite has orthorhombic

perovskite structure. Formation of phase pure LFO by this route is confirmed by the absence of some charactrestic peaks of other phase. The e.ffective crystallite size of LFO considering with strain is 26.7 nm which is calculated from Eq.(1) and confirms by Debye- Scherrer equation

$$D = \frac{K\lambda}{\beta \cos\theta}$$

Where D is crystallite size, K is equal to 0.89 Å , β is FWHM in radians, Cosθ is peak position(2θ/2),θ is the brags angle, ʎ is the X-ray wavelength (0.15406 nm). Total Broadening of peak is due to the combining effect of crystallite size(β) and micro strain(η).

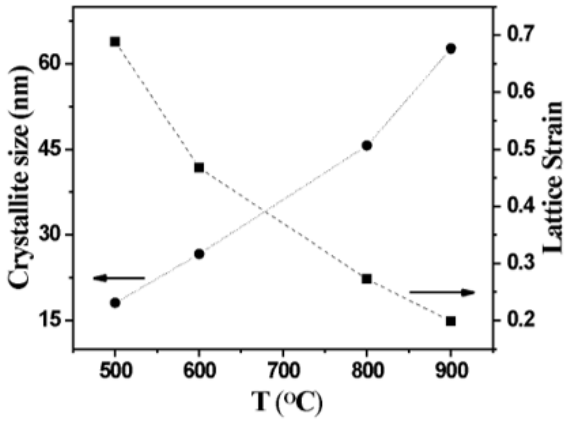


Fig. 1(b): crystallite size and strain on the Full Width Half Maxima(FWHM)

The effect of crystallite size and strain on the Full Width Half Maxima(FWHM) are additive which are expressed by the following equation.

$$\beta\cos\theta/\lambda = 1/d + \eta \sin\theta/\lambda \qquad \text{……..(1)}$$

Result for both microstrain and crystallite size obtained for our samples according to eq.(1) are shown in fig.(2) and a tendency is observed that on increasing calcinations temperature crystallite size increases and micro strain decreases.

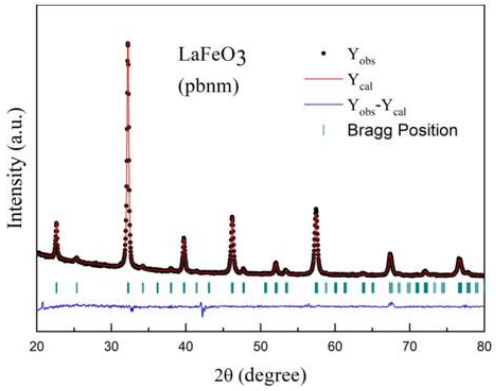
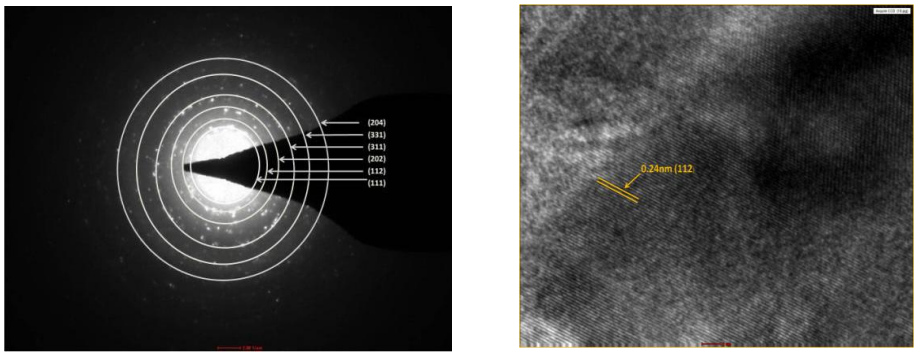


Fig. 2: Rietveld refinement of XRD data for $LaFeO_3$ (LFO) nanoparticles, showing observed (Yobs), calculated (Ycal), difference (Yobs − Ycal) patterns, and Bragg reflections corresponding to the Pbnm space group.

Table 1: Crystallographic parameters, atomic coordinates, Wyckoff positions, and Rietveld refinement reliability factors of $LaFeO_3$.

Space group	Cell parameter	Atoms	Wynkoff position	X	Y	Z	R factor (%)
Pbnm (62)	a=5.0546(5) b = 560(5) c = 7.867(7) α=β=γ= 90°	La Fe O 1 O 2	4c 4b 4c	0.00094 0 -0.04507	0.0244 6 0.5 0.5	0.25 0 0.25	R_p=17.3 R_{wp}=11.4 X^2=1.32



(a) (b)

Fig. 3 (a): shows HRTEM micrograph of LFO powder calcined at 550°C for 2 h. The particles are found to be segregated as observed from figure(b). It is revealed that the synthesized material

The specific diffraction peaks with (101), (111), (121), (210), (112), (220), (131), (202), (212), (103), (311), (123),(331), (242), (143), (204) and (412) diffraction planes with 2θ of 22.65°,25.47°,32.32°,34.28°,38.03°,39.69°,41.56°,46.33°,47.70°,52.03°,53.40°,57.516°,63.79°,67.40°,72.17°,76.78 °,77.87°, correspond to the orthorhombically distorted perovskite structure in LaFeO3 powder samples annealed at 550°C. These diffraction peaks of the $LaFeO_3$ phase are in agreement with JCPDS Card No. 75-0541. A single-phase with pure perovskite structure can be seen in the LaFeO3 powder sample annealed at 550° C. The crystallite sizes (D) of the $LaFeO_3$ powders were estimated from the diffraction peaks using Scherrer's Equation ($D = K\lambda/\beta\cos\theta$), where the K is Scherrer constant (shape factor), k is the x-ray wavelength (1.5418 A˚), β is the full width at half maximum (FWHM) (radians) and θ is Bragg's angle (radians). The K value depends on the crystallite shape and the crystallite size distribution, and it can have values anywhere from 0.62 to 2.08. In this study, K = 0.94 was used and the calculated values of D represent estimates(Lin, Song et al. 2019)

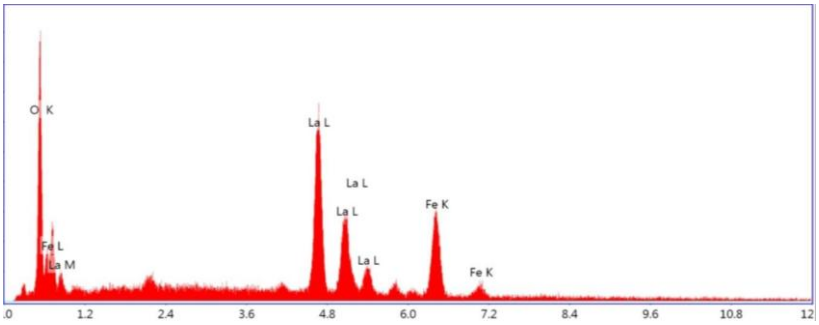


Fig. 4. Energy dispersive spectroscopy (EDS) spectrum of LFO(Lafeo3) nanoparticles.

Table 2: Parameters obtained from the Energy dispersive spectroscopy (EDS)

Element	Weight %	Atomic %	Error %	K ratio
O K	21.23	61.47	7.16	0.14
La L	54.02	18.01	5.28	0.51
Fe k	24.74	20.52	6.25	0.23

consists of nanoparticles with size distribution ranging from 40 to 100 nm. Fig(1b) indicates the homogeneous orientation of the lattice planes with interplanar spacing( ) which correlates with the d spacing value of ( )plane of the system . The selected area electron diffraction pattern (SAED) [Fig. (b)] shows polycrystalline diffraction rings consisting of diffraction spots. The diffraction rings can be indexed as (111), (112), (202), (311), (331), and (204) planes, indicating that LFO nanoparticle has a orthorhombic distorted perovskite structure, which is consistent with the XRD results. EDS spectrum [Fig. (c)] shows the expected elemental signals of La, Fe, and O. We also observed signals of Cu and C which can be ascribed to carbon coated copper grid. The EDS analysis is averaged over three different spots, and the ratio of La/Fe is found to be 0.97:1 within the instrumental accuracy. The ICP spectroscopic measurement of LFO powder exhibits the ratio of La/Fe as 0.99:1 which confirms our EDS results.

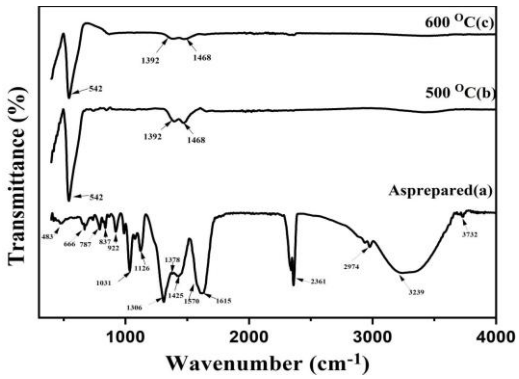


Fig. 5: FT-IR spectrum of $LaFeO_3$ (LFO) nps (a) as prepared sample of LFO (b) calcined at 500ºC (c) calcined at 600ºC

Figure 5 shows the FT-IR spectra of the as prepared LFO precursor powder and precursor powder calcined at 500ºC and 600ºC. The broad adsorption band between 3000-3500 cm^{-1} is assigned to O-H stretching (Taş, Majewski et al. 2000), which decreases in intensity on the increase of thermal-treatment temperature. The intense band located at ~1615 and ~1306 cm^{-1} can be identified as C=O bonds which formed by oxidation of secondary C-OH group of propylene glycol by NO_3^- ions (Stoia, Barvinschi et al. 2012). The strong band located at ~1570 and ~1378 cm^{-1} can be identified to the symmetric (ν_s) and antisymmetric (ν_{as}) vibration of carboxylate (COO^-) group of observed due to oxidation of primary C-OH group of propylene glycol (Prasad, Sulaxna et al. 2005). These carboxylic groups is coordinated to the La^{3+} and Fe^{3+} ions and form carboxylate type complexes. The difference between ν_{as} and ν_s is 192 cm^{-1} which suggest that COO^- group coordinate in monodentate fashion (Zeleňák, Vargová et al. 2007). The band at ~ 1425, 1126 and 1031 cm^{-1} can be assigned to the presence of nitrate ions (Stoia, Barvinschi et al. 2012). In the FT-IR spectrum of the sample calcined at 500ºC for 2.5h, all organic peaks get vanishes and a new IR peak appear at 542 cm^{-1} which is correspond to Fe-O stretching vibration.

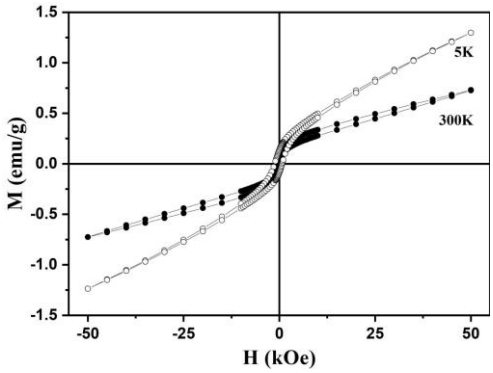


Fig. 5 (a): Magnetic hysteresis loop of $LaFeO_3$ (LFO) nanoparticles calcined at 550ºC

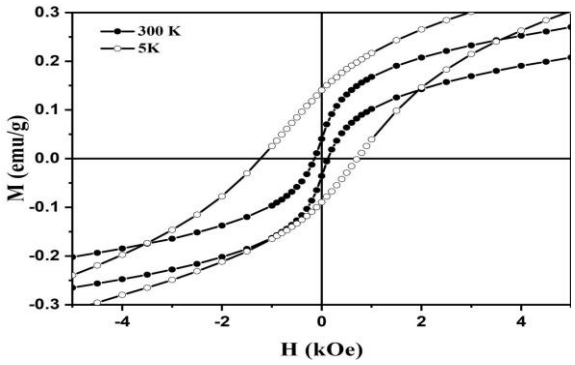


Fig. 5 (b): Magnetic hysteresis loop of $LaFeO_3$ (LFO) nanoparticles calcined at 550^oC

Magnetic properties

The rare earth orthoferrite family of crystal shows ($REFeO_3$) show exceptional magnetic characteristic due to a very little direct magnetic interaction between nearest neighbours Fe^{3+} moment because spins are interconnected through oxygen ions by super exchange interaction mechanisms. Although most of this interaction is antiferromagnetic in nature and it also has an antisymmetric component that results in a weak ferromagnetic moment and a slight canting of the moments of nearby iron atoms. VSM measurement were performed on the nanocrystalline Lanthanum ferric oxide powder sample. M-H curve at low temperature (5K) for $LaFeO_3$ calcined at 550^0C are shown in figure 5 (a), reveals hysteresis loop with magnetic saturation 0.95emu/gm, coercivity1776.6O_e and magnetic remanence 0.062 emu/gm. The hysteresis loop shows characteristic of weak ferromagnetism. At maximum applied field 60K Oe magnetization does not get saturated i.e non saturation of magnetization which is the characteristic of antiferromagnetic behaviour of nanocrystalline $LaFeO_3$ nanoparticles. Generally, lanthanum ferrite shows weak ferromagnetic behaviour or G- type antiferromagnetic with neel temperature above 300K (Ita, Murugavel et al. 2003). It is observed that antiferromagnetic interaction become prominent when nanocrystalline $LaFeO_3$ synthesized using the sol-gel auto combustion process are calcined, the AFM interaction becomes prominent, whereas weak ferromagnetism is shown for LaFeO3 powder that has not been calcined (Qi, Zhou et al. 2003). As La^{3+} ions are nonmagnetic, the magnetic interaction between Fe^{3+} ions and La^{3+}ions are not present. Antiferromagnetic (AFM) coupling occurs in a specific crystallographic direction due to collinear AFM spin order produced by the magnetic super-exchange interactions between the Fe^{3+} ions. Nanocrystalline $LaFeO_3$ shows distorted perovskite type orthorhombic structure due to low symmetry which leads to the tilt of FeO_6 octahedra. Therefore, it can be seen in rise of weak ferromagnetism along another crystallographic direction due to the formation of canted spin order in Fe lattice(Sivakumar, Gedanken et al. 2004 Sivakumar, Gedanken et al. 2004, Shen, Cheng et al. 2009)]. Therefore, both weak ferromagnetism (WFM) and anti-ferromagnetism (AFM) can be seen in the nanocrystalline $LaFeO_3$ systems.

4. Summary and Conclusions

We have successfully synthesized phase pure LFO nanoparticles ranging from 40 to 100 nm by propylene glycol-gel route. XRD indicate that pure perovskite rhombohedral LaFeO3 phase is formed at a temperature as low as 400°C. Moreover, prepared LFO nanopowders have good chemical and compositional homogeneity. LaFeO3 nanoparticles have shown weak ferromagnetic property at room temperature due to size-confinement effects. LaFeO3 nanoparticles have shown strong absorption at ~590 nm arising from the band gap absorption, which may bring some new applications in the area of.

5. Acknowledgements

The measurements were performed at UGC-DAE Consortium for Scientific Research, Indore. Authors are very much thankful to Dr Ram Janay Choudhary UGC-DAE, CSR Indore for valuable discussion.

Referenc:

1. Tugova, E.A., et al., *Phase diagram of the LaFeO3-LaSrFeO4 system.* Glass Physics and Chemistry, 2006. 32(6): p. 674-676.

2. Petrović, S., et al., *LaMO3 (M=Mg, Ti, Fe) perovskite type oxides: Preparation, characterization and catalytic properties in methane deep oxidation.* Applied Catalysis B: Environmental, 2008. 79(2): p. 186-198.
4. Tijare, S.N., et al., *Photocatalytic hydrogen generation through water splitting on nano-crystalline LaFeO3 perovskite.* International Journal of Hydrogen Energy, 2012. 37(13): p. 10451-10456.
5. Wei, Z.-X., et al., *Preparation and catalytic activities of LaFeO3 and Fe2O3 for HMX thermal decomposition.* Journal of Hazardous Materials, 2009. 165(1): p. 1056-1061.
6. Faye, J., et al., *Influence of lanthanum stoichiometry in La1−xFeO3−δ perovskites on their structure and catalytic performance in CH4 total oxidation.* Applied Catalysis B: Environmental, 2012. 126: p. 134-143.
7. Sasikala, C., et al., *Influences of Ti4+ ion on dielectric property in perovskite structure of La ferrite (LaFe1-XTiXO3).* Journal of Alloys and Compounds, 2020. 845: p. 155040.
8. Acharya, S., et al., *Multiferroic behavior of lanthanum orthoferrite (LaFeO3).* Materials Letters, 2010. 64(3): p. 415-418.
9. Sanchez, D.A., et al., *Symmetries and multiferroic properties of novel room-temperature magnetoelectrics: Lead iron tantalate – lead zirconate titanate (PFT/PZT).* AIP Advances, 2011. 1(4).
10. Evans, D.M., et al., *Magnetic switching of ferroelectric domains at room temperature in multiferroic PZTFT.* Nature Communications, 2013. 4(1): p. 1534.
11. Sanchez, D.A., et al., *Room-temperature single phase multiferroic magnetoelectrics: Pb(Fe, M)x(Zr,Ti)(1−x)O3 [M = Ta, Nb].* Journal of Applied Physics, 2013. 113(7).
12. Evans, D.M., et al., *Switching ferroelectric domain configurations using both electric and magnetic fields in Pb (Zr, Ti) O3–Pb (Fe, Ta) O3 single-crystal lamellae.* Philosophical Transactions of the Royal Society A: Mathematical, Physical and Engineering Sciences, 2014. 372(2009): p. 20120450.
13. Schiemer, J., et al., *Studies of the room-temperature multiferroic Pb (Fe0. 5Ta0. 5) 0.4 (Zr0. 53Ti0. 47) 0.6 O3: resonant ultrasound spectroscopy, dielectric, and magnetic phenomena.* Advanced functional materials, 2014. 24(20): p. 2993-3002.
14. Glinchuk, M.D., E.A. Eliseev, and A.N. Morozovska, *Novel room temperature multiferroics on the base of single-phase nanostructured perovskites.* Journal of Applied Physics, 2014. 116(5).
15. Glinchuk, M.D., E.A. Eliseev, and A.N. Morozovska, *Landau-Ginzburg description of anomalous properties of novel room temperature multiferroics Pb (Fe1/2Ta1/2) x (Zr0. 53Ti0. 47) 1-xO3 and Pb (Fe1/2Nb1/2) x (Zr0. 53Ti0. 47) 1− xO3.* Journal of Applied Physics, 2016. 119(2).
16. Liu, J.M., et al., *Order coupling in ferroelectromagnets as simulated by a Monte Carlo method.* Physical Review B, 2002. 66(5): p. 054416.
17. Dann, S.E., et al., *The Effect of Oxygen Stoichiometry on Phase Relations and Structure in the System La1-xSrxFeO3-δ (0 ≤ x ≤ 1, 0 ≤ δ ≤ 0.5).* Journal of Solid State Chemistry, 1994. 109(1): p. 134-144.
18. Koehler, W.C. and E.O. Wollan, *Neutron-diffraction study of the magnetic properties of perovskite-like compounds LaBO3.* Journal of Physics and Chemistry of Solids, 1957. 2(2): p. 100-106.
19. Hearne, G.R., et al., *Electronic structure and magnetic properties of ${\mathrm{LaFeO}}_{3}$ at high pressure.* Physical Review B, 1995. 51(17): p. 11495-11500.
20. Bhalla, A., R. Guo, and R. Roy, *The perovskite structure—a review of its role in ceramic science and technology.* Materials research innovations, 2000. 4(1): p. 3-26.
21. Sun, J., G. Rao, and J. Liang, *Crystal structure and electronic transport property of perovskite manganese oxides with a fixed tolerance factor.* Applied physics letters, 1997. 70(14): p. 1900-1902.
22. Ye, J., et al., *Dielectric properties of ErFeO3 ceramics over a broad temperature range.* Journal of alloys and compounds, 2014. 617: p. 850-854.
23. Chanda, S., et al., *Multiferroicity in La1/2Nd1/2FeO3 nanoparticles.* Solid state sciences, 2014. 37: p. 55-63.
24. Prasad, B.V., et al., *Colossal dielectric constant in PrFeO3 semiconductor ceramics.* Solid State Sciences, 2012. 14(2): p. 225-228.
25. Xia, W., et al., *Colossal dielectric behavior in TbFeO3 ceramics.* Current Applied Physics, 2013. 13(8): p. 1743-1745.
26. Idrees, M., et al., *Phase structure, microstructure and dielectric properties of (K0. 5Na0. 5) NbO3-LaFeO3 high-temperature dielectric ceramics.* Acta Mater, 2011. 59: p. 1338-1345.
27. Ivanov, S.A., et al., *Preparation, structural, dielectric and magnetic properties of LaFeO3–PbTiO3 solid solutions.* Materials Research Bulletin, 2012. 47(11): p. 3253-3268.
28. Song, P., et al., *The structure, electrical and ethanol-sensing properties of La1− xPbxFeO3 perovskite ceramics with x≤ 0.3.* Sensors and Actuators B: Chemical, 2005. 104(2): p. 312-316.
29. Zheng, W., et al., *Hydrothermal synthesis of LaFeO3 under carbonate-containing medium.* Materials Letters, 2000. 43(1): p. 19-22.

30. Thirumalairajan, S., et al., *Controlled synthesis of perovskite LaFeO3 microsphere composed of nanoparticles via self-assembly process and their associated photocatalytic activity.* Chemical Engineering Journal, 2012. 209: p. 420-428.
31. Nakayama, S., *LaFeO3 perovskite-type oxide prepared by oxide-mixing, co-precipitation and complex synthesis methods.* Journal of materials science, 2001. 36: p. 5643-5648.
32. Kumar, M., et al., *Synthesis of pure and Sr-doped LaGaO3, LaFeO3 and LaCoO3 and Sr,Mg-doped LaGaO3 for ITSOFC application using different wet chemical routes.* Materials Chemistry and Physics, 2009. 113(2): p. 803-815.
33. Matei, C., et al., *Synthesis of lanthanum ferrite nanopowder by combustion method.* Journal of optoelectronics and advanced materials, 2007. 9(6): p. 1793-1796.
34. Köferstein, R., L. Jäger, and S.G. Ebbinghaus, *Magnetic and optical investigations on LaFeO3 powders with different particle sizes and corresponding ceramics.* Solid State Ionics, 2013. 249-250: p. 1-5.
35. Bellakki, M.B., B.J. Kelly, and V. Manivannan, *Synthesis, characterization, and property studies of (La, Ag) FeO3 (0.0≤x≤0.3) perovskites.* Journal of Alloys and Compounds, 2010. 489(1): p. 64-71.
36. Tang, P., et al., *Microwave-assisted synthesis of nanoparticulate perovskite LaFeO3 as a high active visible-light photocatalyst.* Current Applied Physics, 2013. 13(2): p. 340-343.
37. Farhadi, S., Z. Momeni, and M. Taherimehr, *Rapid synthesis of perovskite-type LaFeO3 nanoparticles by microwave-assisted decomposition of bimetallic La[Fe(CN)6]·5H2O compound.* Journal of Alloys and Compounds, 2009. 471(1): p. L5-L8.
38. Sivakumar, M., et al., *Sonochemical synthesis of nanocrystalline LaFeO 3.* Journal of Materials Chemistry, 2004. 14(4): p. 764-769.
39. Kindermann, L., et al., *Influence of iridium on the reactivity of LaFeO3 base perovskites.* Solid State Ionics, 1998. 106(1): p. 165-172.
40. Liu, X., et al., *Preparation and acetone sensitive characteristics of nano-LaFeO3 semiconductor thin films by polymerization complex method.* Materials Science and Engineering: B, 2006. 133(1): p. 98-101.
41. Giannakas, A.E., A.K. Ladavos, and P.J. Pomonis, *Preparation, characterization and investigation of catalytic activity for NO+CO reaction of LaMnO3 and LaFeO3 perovskites prepared via microemulsion method.* Applied Catalysis B: Environmental, 2004. 49(3): p. 147-158.
42. Chung, S.-H., K.-C. Chiu, and J.-H. Jean, *Preparation and electrical properties of LaFeO3 compacts using chemically synthesized powders.* Japanese journal of applied physics, 2008. 47(11R): p. 8498.
43. Gu, F., et al., *Photoluminescence Properties of SnO2 Nanoparticles Synthesized by Sol−Gel Method.* The Journal of Physical Chemistry B, 2004. 108(24): p. 8119-8123.
44. Rietveld, H.M., *A profile refinement method for nuclear and magnetic structures.* Journal of applied Crystallography, 1969. 2(2): p. 65-71.
45. Rodríguez-Carvajal, J., *Recent advances in magnetic structure determination by neutron powder diffraction.* Physica B: Condensed Matter, 1993. 192(1-2): p. 55-69.
46. Taş, A.C., P.J. Majewski, and F. Aldinger, *Chemical Preparation of Pure and Strontium- and/or Magnesium-Doped Lanthanum Gallate Powders.* Journal of the American Ceramic Society, 2000. 83(12): p. 2954-2960.
47. Stoia, M., et al., *Synthesis of nanocrystalline nickel ferrite by thermal decomposition of organic precursors.* Journal of thermal analysis and calorimetry, 2012. 108(3): p. 1033-1039.
48. Prasad, R., Sulaxna, and A. Kumar, *Kinetics of thermal decomposition of iron (III) dicarboxylate complexes.* Journal of thermal analysis and calorimetry, 2005. 81(2): p. 441-450.
49. Zeleňák, V., Z. Vargová, and K. Györyová, *Correlation of infrared spectra of zinc (II) carboxylates with their structures.* Spectrochimica Acta Part A: Molecular and Biomolecular Spectroscopy, 2007. 66(2): p. 262-272.
50. Lin, L., et al., *Enhanced As(III) removal from aqueous solution by Fe-Mn-La-impregnated biochar composites.* Science of The Total Environment, 2019. 686: p. 1185-1193.
51. Hunpratub, S., et al., *Optical and magnetic properties of La1− xGaxFeO3 nanoparticles synthesized by polymerization complex method.* Applied Surface Science, 2016. 380: p. 52-59.
52. Yang, Z., et al., *Controlled synthesis of highly ordered LaFeO3 nanowires using a citrate-based sol–gel route.* Materials Research Bulletin, 2006. 41(2): p. 274-281.
53. Cho, Y.-G., et al., *Characterization and catalytic properties of surface La-rich LaFeO3 perovskite.* Bull Korean Chem Soc, 2009. 30(6): p. 1368-1372.
54. Lee, W.-Y., H.J. Yun, and J.-W. Yoon, *Characterization and magnetic properties of LaFeO3 nanofibers synthesized by electrospinning.* Journal of Alloys and Compounds, 2014. 583: p. 320-324.
55. Guan, S., et al., *Preparation and promising application of novel LaFeO3/BiOBr heterojunction photocatalysts for photocatalytic and photo-Fenton removal of dyes.* Optical Materials, 2020. 100: p. 109644.

56. Signorelli, A. and R. Hayes, *X-ray photoelectron spectroscopy of various core levels of lanthanide ions: the roles of monopole excitation and electrostatic coupling.* Physical Review B, 1973. 8(1): p. 81.
57. Bilgin Simsek, E., Ö. Tuna, and Z. Balta, *Construction of stable perovskite-type LaFeO3 particles on polymeric resin with boosted photocatalytic Fenton-like decaffeination under solar irradiation.* Separation and Purification Technology, 2020. 237: p. 116384.
58. Ita, B., et al., *Magnetic properties of lanthanum orthoferrite fine powders prepared by different chemical routes.* Journal of Chemical Sciences, 2003. 115: p. 519-524.
59. Qi, X., et al., *Auto-combustion synthesis of nanocrystalline LaFeO3.* Materials Chemistry and Physics, 2003. 78(1): p. 25-29.
60. Shen, H., et al., *Combustion synthesis and characterization of nano-crystalline LaFeO3 powder.* physica status solidi (a), 2009. 206(7): p. 1420-1424.